www.czasopisma.pan.pl PAN POLSKA AKADEMIA NAUK www.journals.pan.pl

ARCHIVES OF ACOUSTICS Vol. 49, No. 4, pp. 613–624 (2024), doi: 10.24425/aoa.2024.148803

Research Paper

An Algorithm for Ultrasonic Identification of Ceramic Materials and Virtual Prototype Realization

Yu LIU(1), XiPing HE(1)*, ShengPing HE(2)

(1) *Shaanxi Key Laboratory of Ultrasonic, School of Physics and Information Technology*
Shaanxi Normal University
Xi'an, China

(2) *High-Tech. Institute*
Sichuan, Luzhou, China

*Corresponding Author e-mail: Hexiping@snnu.edu.cn

(*received October 24, 2020; accepted April 2, 2020; published online July 5, 2024*)

To prevent important items from being replaced by a forgery, an ultrasonic fingerprint identification algorithm is proposed and an identification program is developed. A virtual prototype for the ultrasonic identification of ceramics is developed based on an ultrasonic detection card. This virtual prototype allows for the simultaneous transmission and acquisition of signals. Numerous experimental tests were conducted using this virtual prototype. The results demonstrate that the virtual prototype achieves accurate identification of ceramics. This virtual prototype lays a good foundation for the development of intelligent, automated, integrated, and miniaturized ultrasonic identification systems.

Keywords: ceramic material; ultrasonic testing; ultrasonic scattering; ultrasonic fingerprint; virtual prototype.

1. Introduction

In recent years, with the continuous progress of technology, the number of counterfeit ceramics has been increasing, and anti-counterfeiting technology is facing a great challenge. Resonance acoustic spectroscopy has been used at the Los Alamos National Laboratory, USA, to safely monitor nuclear containers of UF_6 and to inspect whether nuclear containers or chemical weapons have been tampered with (OLINGER *et al.*, 1993). Traditional ceramic identification mainly relies on organoleptic assessment, such as touching, observing, and smelling. Many counterfeit ceramics are difficult to identify by traditional methods due to the limitations of human sensory organs. Therefore, the issue of how to identify ceramics has been a concern of scholars.

There are many reports on identification methods for ceramics, including the use of X-ray diffraction, chemical element labeling, and X-ray computed tomography image reconstruction. In these methods, X-rays are transmitted through the object to be detected and imaged on photographic film or recorded on a digital sensor. The objects can be identified according to the information presented in the image. However, there are two shortcomings to these methods: the impact of radiation on human health and radiation pollution (DEJOIE *et al.*, 2015; SCIAU *et al.*, 2011; PADELETTI *et al.*, 2010; FIGUEIREDO *et al.*, 2010).

In the current study, ultrasonic detection technology is used to identify ceramics. This method not only overcomes the limitations of traditional methods but also is not harmful to human health or the environment. All one needs to do is fix an ultrasound probe onto the surface of the object to be identified. The operating steps are more convenient and safer compared to traditional methods. In addition, the technology has many advantages, such as low cost, excellent discrimination, and high accuracy (SHI *et al.*, 2015).

The scattering of ultrasonic waves in contact with grains and interfaces in polycrystalline materials results in attenuation and dispersive velocities (BADIDI *et al.*, 2003). Random ultrasonic backscattering results from the random orientation distribu-

tion, shape, size, and interface of the grains. Moreover, the ultrasonic velocity is explicitly related to grain size. Palanichamy *et al.* (1995) estimated the average grain size in austenitic stainless steel using ultrasonic velocity measurements and obtained more accurate results compared to attenuation measurements. The attenuation of ultrasonic waves is closely related to the distribution of grains in polycrystalline materials. Even if the average grain size is the same for two different-shaped grains, their internal ultrasonic attenuation will be significantly different (Smith, 1982).

An analytical equation to explain the relationship between backscattering and microtexture size and orientation has been proposed. The numerical result of this equation is consistent with the result measured using orientation image microscopy. In addition, research on the ultrasonic backscatter coefficient has clarified the complex interrelationship between polycrystalline grains and ultrasonic waves (Sarpün *et al.*, 2005). The microstructure of polycrystalline materials determines the ultrasonic velocity, attenuation, and backscatter power of ultrasonic waves propagating inside the material (Laux *et al.*, 2002; Hirao *et al.*, 1987; Özkan *et al.*, 2013; Vijayalakshmi *et al.*, 2011; Murthy *et al.*, 2008). Conversely, ultrasound can also effectively characterize the difference in the internal microstructure of polycrystalline materials. Each finished material in industrial production has unique microstructural characteristics, just like human fingerprints. Using ultrasonic fingerprint technology to prevent valuables from being replaced has been a new application in the field of ultrasonic testing in recent years. When ultrasonic waves propagate in an object, the scattering signal is highly correlated with its internal structure (Li *et al.*, 2014; Buenos *et al.*, 2014).

In this study, scattering signals of three ceramic disks of identical material and appearance are extracted using an ultrasonic probe with a frequency of 5 MHz, and the ultrasonic fingerprints of the signals are extracted to identify the ceramic specimens.

2. Identification algorithm

Ultrasonic reflection signals and scattering signals are acquired from the ceramics that need to be protected. The features of the signals are processed to calculate the "target ultrasonic fingerprint". When ceramics with the same appearance are mixed, the ultrasonic signals are acquired from each specimen, respectively. After processing the signals acquired by the virtual prototype, features are extracted from the signal of each specimen, and the ultrasonic fingerprints to be identified are calculated based on these features. The identification is completed by comparing the "fingerprints to be identified" with the "target ultrasonic fingerprint". This process involves both time-domain identification and frequency-domain identification. Whether the ceramic to be identified is the target ceramic is determined according to the identification results of the ultrasonic fingerprints.

First, to reduce the effect of errors and improve anti-interference capability, the acquired time-domain signals are normalized using:

$$A_n = \frac{X_n - X_{\min}}{X_{\max} - X_{\min}}, \tag{1}$$

where $X_{\min}$ is the minimum amplitude of the signal, $X_{\max}$ is the maximum amplitude, and X_n and A_n are, respectively, the amplitude of each sampling point before and after normalization (where $n = 1, 2, 3, ..., N$).

Second, a parameter P_i (where $i = 1, 2, 3, ..., 20$) is defined as follows:

$$P_i = \frac{A_n}{\sqrt{\sum_{n=1}^{N} A_n^2}}. \tag{2}$$

Twenty sets of signals were acquired as target signals in each experiment to reduce operational and systematic errors. Therefore, there are 20 sets of P_i. Subsequently, the arithmetic mean P_v was calculated based on P_i. The feature of each target time-domain signal F_i was calculated according to:

$$F_i = \sum_{n=1}^{N} \left| \ln \frac{P_i}{P_v} \right|. \tag{3}$$

The target signal features in the frequency domain are similar to those in the time domain, with the difference being that A_n is obtained using a fast Fourier transform after Eq. (1). P_i is calculated by using the frequency spectrum of A_n in Eq. (2), and the features in the frequency domain can be calculated by using Eq. (3). Finally, there is one feature in the time domain and one feature in the frequency domain, obtained by averaging the features of the 20 sets of signals. These two features are, respectively, the ultrasonic fingerprints in the time and frequency domains.

The steps for extracting the ultrasonic fingerprints of the signals to be identified are similar to those used for the target signals. It is worth noting that P_v of the signals to be identified is still the value while calculating the target signal features. This means that the fingerprint to be identified is calculated based on the target fingerprint. The fingerprint to be identified indicates the dissimilarity compared to the target fingerprint. The ultrasonic fingerprints in the time and frequency domains need to be compared with the target signal ultrasonic fingerprints, respectively, to improve the accuracy of the identification. Although the target ultrasonic fingerprints and the ultrasonic fingerprints to be identified have been obtained from the identical ceramic, they will differ somewhat under actual conditions because of inevitable errors such as operating error and system noise. Therefore, it is necessary to

calculate a threshold. The variation of signal amplitude caused by error is a random variable with independent distribution. In statistical analysis, all signals that may be collected are statistical populations, while the signals collected from the populations are statistical samples. According to the central limit theorem, the distribution of the sample mean will approximate a Gaussian distribution, regardless of the population distribution. Therefore, it is feasible to judge the outliers by using the Pauta criterion.

In statistics, three times the value of the standard deviation is considered as a reasonable margin of error and measurements beyond the reasonable margin of error are identified as outliers. Therefore, the standard deviation can be calculated by using:

$$\sigma = \sqrt{\frac{\sum_{i=1}^{k} (\overline{F} - F_k)^2}{k}}, \tag{4}$$

where $\overline{F}$ is the mean value of the target signal ultrasonic fingerprints and k is the number of target signals ($k = 20$ in this study). The threshold Q is then given as:

$$Q = \overline{F} + 3\sigma. \tag{5}$$

Therefore, according to the Pauta criterion, the probability of a deviation greater than 3σ is ~0.0026, which is a rare probability event.

The result of the identification is obtained by assessing whether the ultrasonic fingerprints to be identified are within the range of the threshold.

3. Experimental instruments

In this study, four ceramic plates of the same shape and material were used as specimens, as shown in Fig. 1. Each of the plates had a diameter of 175 mm and a bottom thickness of 5 mm. The velocity of ultrasound in the plates was 6250 m/s. The velocity of ultrasound propagation in the 5 mm thick plate was obtained by measuring the time difference between the first and second ultrasonic echoes. A dark blue plastic sheet cut at right angles was pasted on the surface of the ceramic plate. The position of the probe was determined when the right angle sides of the plastic slice were tangent to circular probe. The plastic sheet plays an important role in accurately fixing the probe position.

Fig. 1. Right-angle positioner and specimens.

Figure 2 shows the ultrasonic flaw detection card (CTS-04PC) customized from Shantou Ultrasonic Electronics Company (China). This model of ultrasonic flaw detection card is available for Peripheral Component Interconnect (PCI) slots and ultrasonic probes. The function of the card depends on the operating status of the registers. The computer controls the base address and offset of the registers to control the working mode of the ultrasonic flaw detection card. Therefore, the probe is connected to the ultrasonic flaw detection card, which is then assembled in the PCI slot of the computer. Together, all these components form a virtual prototype, as shown in Fig. 3.

Fig. 2. Ultrasonic flaw detection card.

Fig. 3. Virtual prototype.

The internal structure of the virtual prototype is shown in Fig. 4. The operational program for the ultrasonic flaw detection card was written in C++. The sampling frequency of the system was 100 MHz, and the excitation waveform consisted of a positive half-wave, a negative half-wave, and a radio-frequency wave. The excitation voltage could be regulated from 0 V to 300 V, and the gain range could be adjusted from 0 dB to 110 dB. The pulse repetition rate was 10 kHz. Damping, ultrasonic velocity, display range of the waveform, and other parameters can all be adjusted according to actual conditions.

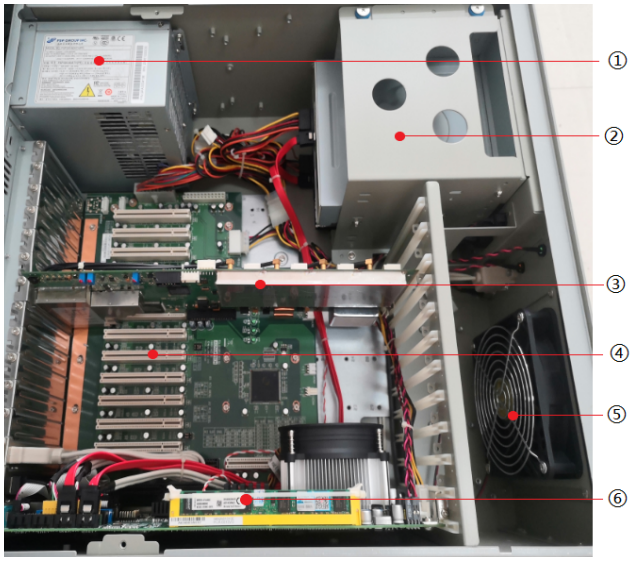

Fig. 4. Internal structure of the virtual prototype: 1) a PC power supply unit; 2) an optical disk driver; 3) an ultrasonic flaw detection card; 4) PCI slots; 5) a cooling fan; 6) a computer motherboard.

4. Identification of ceramics and results

4.1. Microstructure of ceramics

Cross-sectional scanning electron microscope (SEM) images of three ceramic specimens studied during the experiment are shown in Figs. 5a–c. The sizes, shapes, and interfaces of the ceramic microtextures are all quite different. According to the SEM results, the granularity of the ceramics used in the experiments ranges from 0.05 μm to 0.3 μm. These grains are arranged in a disorganized manner, and the boundaries between the particles are not clear. The SEM images show that the internal microstructure of different portions of the same ceramic sample also varies greatly.

The interaction between ultrasonic waves and the ceramic material is closely related to the wavelength of ultrasound and the size of the ceramic particles. The wavelength λ of the 5 MHz ultrasonic waves used in the experiment is 1.2 mm inside the ceramic sample, and the particle sizes of ceramics are in the range

a)

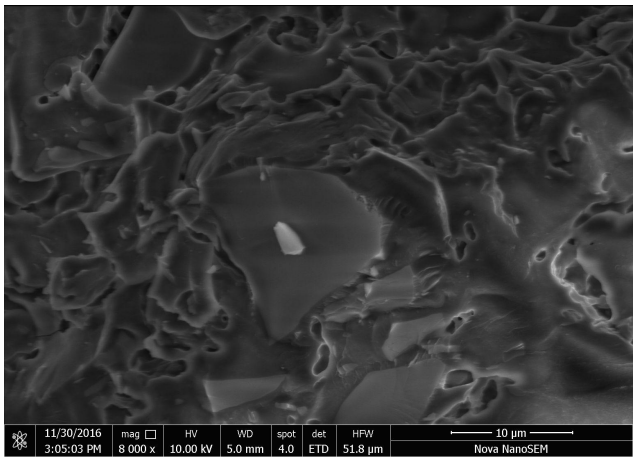

b)

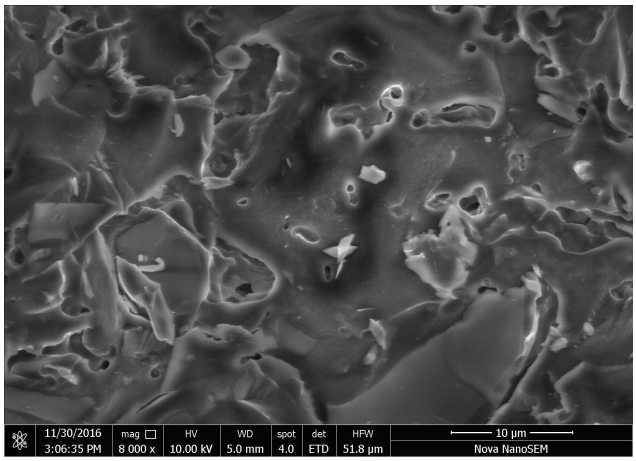

c)

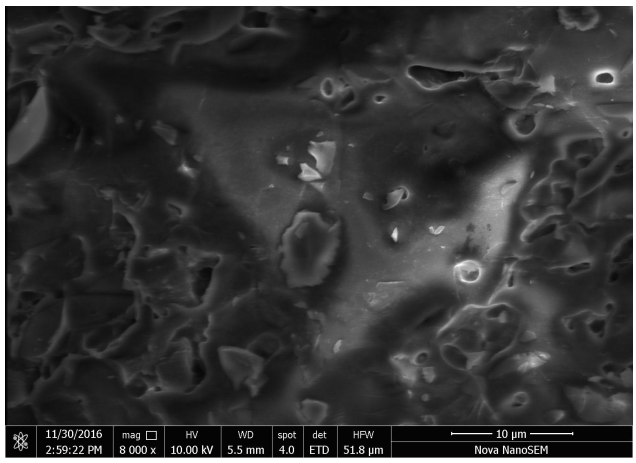

Fig. 5. SEM images of ceramic cross-sections.

of 0.5 μm~3 μm. The wavelength is much larger than the particle sizes, satisfying the condition for Rayleigh scattering. The scattering coefficient is proportional to the fourth power of the frequency, meaning higher frequency is conducive to improving the intensity of scattering signals and extracting more features from the specimens (Yang *et al.*, 2012). Because of the irregular structure inside ceramics, the scattered waves generated by identical parts of different ceramics vary, and consequently, the characteristics of the scattered signals received by the probe also differ, which is the basis for identifying the ceramic samples.

4.2. Identification steps

Firstly, signals were acquired from the samples to be protected using an ultrasonic probe and saved by the virtual prototype. Secondly, ultrasonic signals from all the samples were extracted using the same ultrasonic probe and saved as additional data. Thirdly, features of the target ultrasound fingerprints were calculated in both time and frequency domains. In this way, these feature thresholds were then obtained and saved as the "target ultrasonic fingerprint". Fourthly, features of the ultrasonic fingerprints to be identified were calculated in both time and frequency domains and saved as the "ultrasonic fingerprint to be identified". Finally, results were obtained according to the relationship between the features of "ultrasonic fingerprint to be identified" and the "target ultrasonic fingerprint".

If the features of the "ultrasonic fingerprint to be identified" fall below the thresholds in both time and frequency domains, the result is "same item". If the features are above the thresholds in both time and frequency domains, the result is "different item". However, if the features are below the threshold in one domain and above it in another, the result is "uncertain".

Increasing the number of signal acquisition makes the distribution of signals more stable and improves the accuracy of identification. Target signals should be acquired in 20 sets, while signals to be identified should be acquired in more than 5 sets based on previous experience. The result with the highest frequency of occurrences is the final result. If the result is "uncertain", the signal to be identified needs to be re-extracted until a clear result is obtained.

4.3. Identification of ceramic specimens

The first step involves configuring the parameters of the virtual prototype by, for example, setting the ultrasonic velocity according to the specimen material. The frequency of the excitation signal is 5 MHz. The sampling time should be adjusted to ensure the number of the ultrasonic echoes is more than 5. In this study, a sampling time of 20 μs is sufficient for the samples. It should be noticed that varying sampling time will lead to different signal acquisitions. For consistent identification of a specific item, the sampling time must remain consistent in all signal acquisitions.

The second step includes adjusting the gain based on the amplitude feature of the specimen. Ultrasonic wave signals in various materials are different. Adjusting the gain settings according to the specific material features is beneficial to improve identification accuracy. The upper limit of the amplitude of the virtual prototype is 250 V, and it is important to avoid an amplitude exceeding this limit during gain adjustment.

The third step involves signal acquisition. Making sure a probe is placed in the same position each time is important because signals vary in different probe's positions, even when they are from the same specimen.

Eventually, water is used as the coupling agent. It is crucial to keep the bottom of the specimen dry because ultrasonic waves pass through the coupling agent to reach the bottom of the specimen, where they reflect off the surface on which the specimen is placed.

The experimental specimens were four ceramic disks made from the same material and having identical appearance, as shown in Fig. 1. The specimens were labeled as 1–4. Specimen #1 was designated as the target specimen. Twenty sets of ultrasonic signals were acquired for the target specimen (#1), while seven sets were acquired for every specimen to be identified (#1, #2, #3, and #4). These signals were processed to obtain ultrasonic fingerprints. The time-domain signals of the ceramic specimens are shown in Fig. 6. A comparison of the amplitudes of these time-domain signals clearly shows that the ultrasonic signals of these specimens varied significantly. Although the waveforms of specimens #3 and #4 appear similar, the details differed enormously, which could be identified by ultrasonic fingerprints.

The ultrasonic fingerprints of the target specimen (#1) are listed in Table 1. The ultrasonic fingerprints to be identified of specimens #1 and #2 are listed in Tables 2 and 3, respectively. For brevity, partial data in Table 1 have been omitted. The ultrasonic fingerprints for specimens #3 and #4 are not included in this study as their results were similar to specimen #2 when compared with the target specimen (#1). The results of the identification experiment for each specimen are given in Table 4.

The arithmetic mean $\overline{F}$ and standard deviation σ of the target ultrasonic fingerprints are calculated from Table 1. Subsequently, thresholds in the time and frequency domains are obtained using Eq. (5). These thresholds are given in Tables 2 and 3 to compare with the ultrasonic fingerprints to be identified. Table 2 indicates that six of the seven ultrasonic fingerprints to be identified for specimen #1 fell below the thresholds in both time and frequency domains. Only the third ultrasonic fingerprint could not be identified as the "same item" because the ultrasonic fingerprint value in the

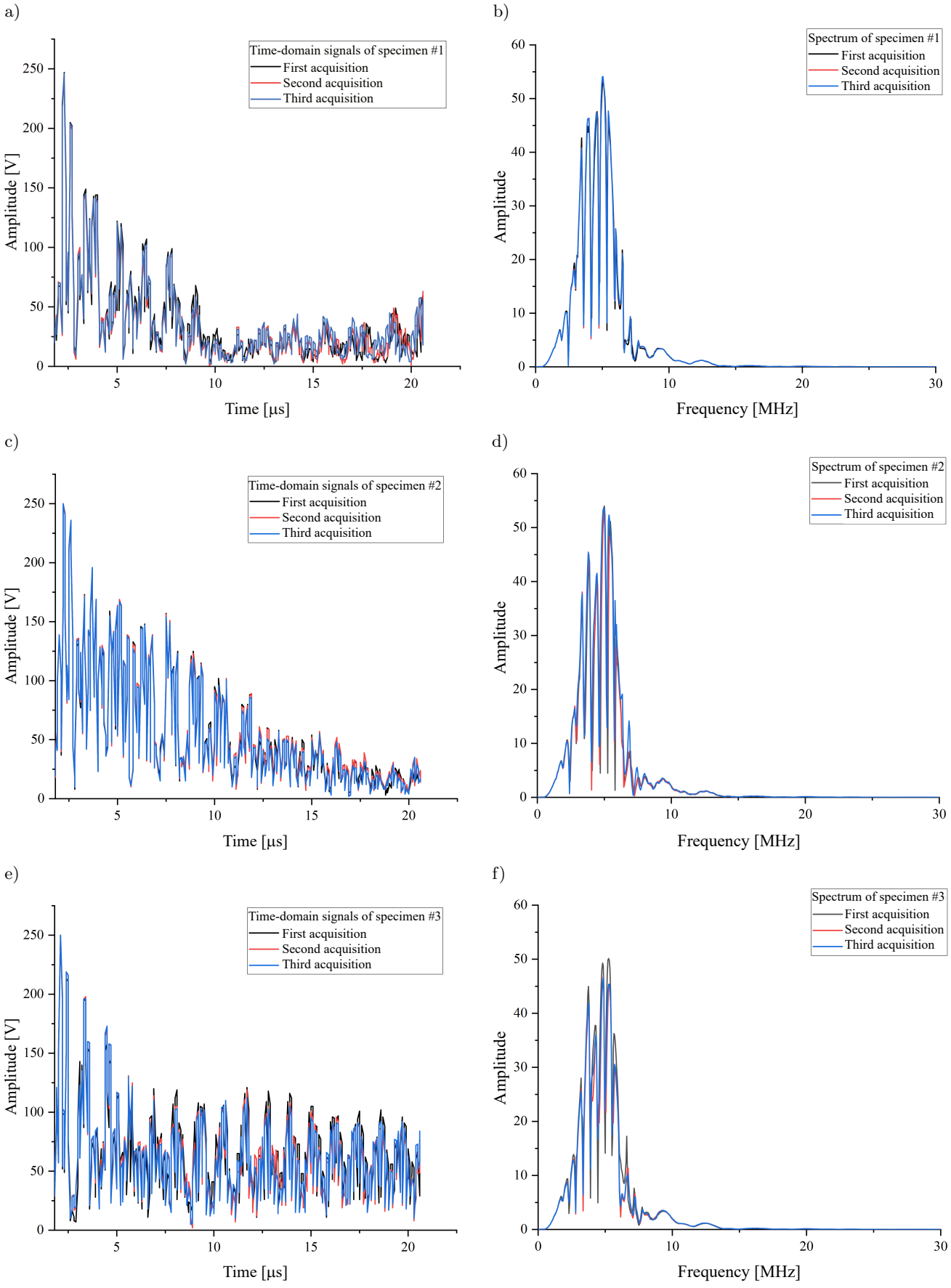
a)
Time-domain signals of specimen #1
First acquisition
Second acquisition
Third acquisition
Amplitude [V]
Time [μs]
b)
Spectrum of specimen #1
First acquisition
Second acquisition
Third acquisition
Amplitude
Frequency [MHz]
c)
Time-domain signals of specimen #2
First acquisition
Second acquisition
Third acquisition
Amplitude [V]
Time [μs]
d)
Spectrum of specimen #2
First acquisition
Second acquisition
Third acquisition
Amplitude
Frequency [MHz]
e)
Time-domain signals of specimen #3
First acquisition
Second acquisition
Third acquisition
Amplitude [V]
Time [μs]
f)
Spectrum of specimen #3
First acquisition
Second acquisition
Third acquisition
Amplitude
Frequency [MHz]

[Fig. 6a-f.].

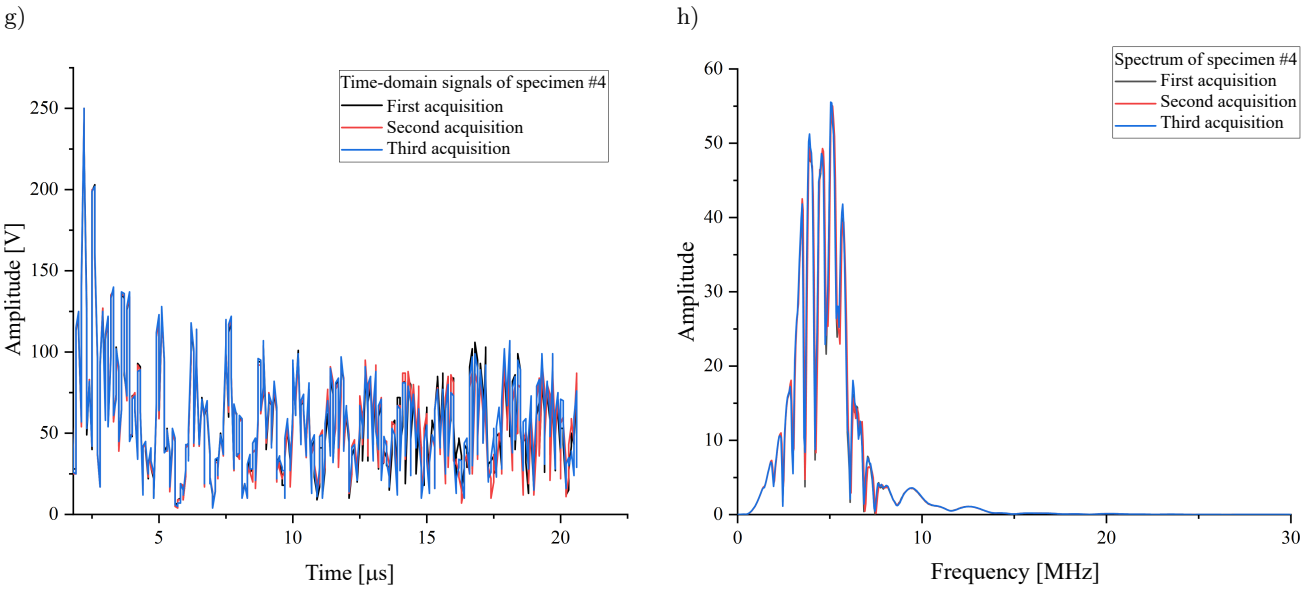

Fig. 6. Time-domain signals and spectra of the specimens at the same position.

Table 1. Target ultrasonic fingerprints of specimen #1.

Domain	Number							
	1	2	3	4	5	...	19	20
Time	4.0507	3.2753	3.8776	3.7949	4.3667	...	4.4440	3.4480
Frequency	24.0818	20.5954	25.5155	25.2757	26.1027	...	28.4524	23.4338

Table 2. Identification of specimen #1 by using ultrasonic fingerprints.

Domain	Number							Threshold
	1	2	3	4	5	6	7	
Time	4.0275	4.5044	6.1990	4.9447	5.0663	4.6045	4.8150	6.1483
Frequency	27.8061	26.4829	31.1543	26.9516	27.7434	28.6894	26.8546	36.6512

Table 3. Identification of specimen #2 by using ultrasonic fingerprints.

Domain	Number							Threshold
	1	2	3	4	5	6	7	
Time	18.4371	18.3059	18.1403	18.4292	18.5042	18.4900	18.4638	6.1483
Frequency	74.2805	72.5703	72.1178	71.8594	72.0542	73.1422	71.8704	36.6512

Table 4. Identification of each specimen by using ultrasonic fingerprints.

Identification specimen	#1 identifies				#2 identifies				#3 identifies				#4 identifies			
	#1	#2	#3	#4	#1	#2	#3	#4	#1	#2	#3	#4	#1	#2	#3	#4
Same	6	0	0	0	0	6	0	0	0	0	7	0	0	0	0	6
Different	0	7	7	7	7	0	7	7	7	7	0	7	7	7	7	0
Result	Same	Different	Different	Different	Different	Same	Different	Different	Different	Different	Same	Different	Different	Different	Different	Same

frequency domain was lower than the threshold while its time domain value was higher than the threshold. Therefore, the result for the third ultrasonic fingerprint was identified as "uncertain". With 6 results indicating "same item" and 0 indicating "different item", the final identification for specimen #1 was concluded as "same item".

Table 3 indicates that ultrasonic fingerprints to be identified for specimen #2 are much higher than both the time and frequency thresholds. Obviously,

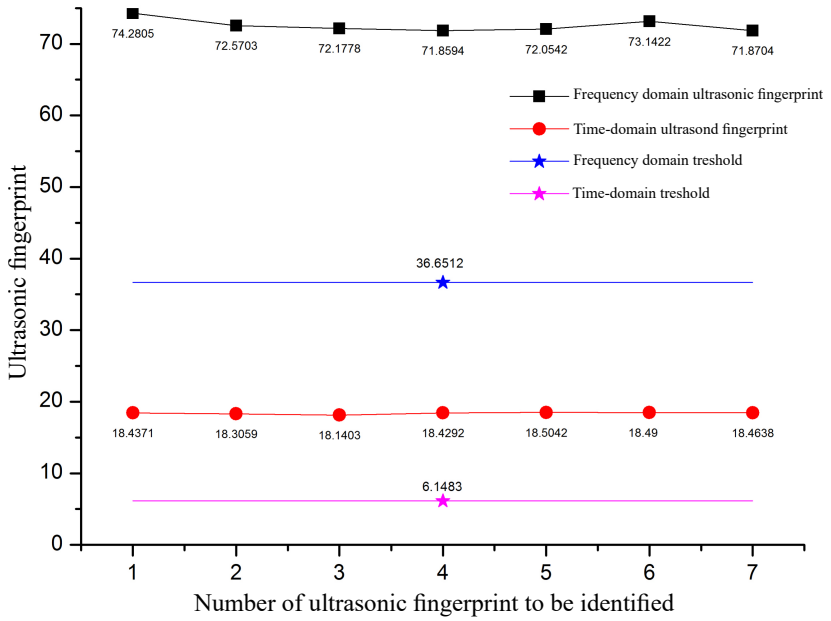

Fig. 7. Ultrasonic fingerprints of specimen #2.

all these seven ultrasonic fingerprints are identified as "different items". The relationship between ultrasonic fingerprints and their respective thresholds is plotted in Fig. 7. Furthermore, the ultrasonic fingerprints of the four samples were treated as target ultrasonic fingerprints in the proper sequence and then identified with each other. As presented in Table 4, each ceramic sample was accurately identified even when they were mixed up.

4.4. Experiments on other specimens

In addition to the ceramic plate specimens, we also performed experimental verification on three ceramic boxes, three ceramic sinks, and three round ceramic pots, as shown in Fig. 8. The sinks had a length of 53 cm, a width of 38 cm, a depth of 53 cm, and a thickness of 10 mm. The boxes had a length of 53 mm, a width of 53 mm, and a bottom thickness of 5 mm. The pots had a diameter of 58 mm and a bottom thickness of 3 mm.

The ceramic sinks were labeled as 5–7. Specimen #5 was designated as the target specimen. The time-domain signals and spectra of the ceramic sinks are shown in Fig. 9.

The ultrasonic fingerprints of the target specimen (#5) are listed in Table 5. The ultrasonic fingerprints to be identified for specimens #5 and #6 are listed in Tables 6 and 7, respectively. For brevity, partial data in Table 5 have been omitted.

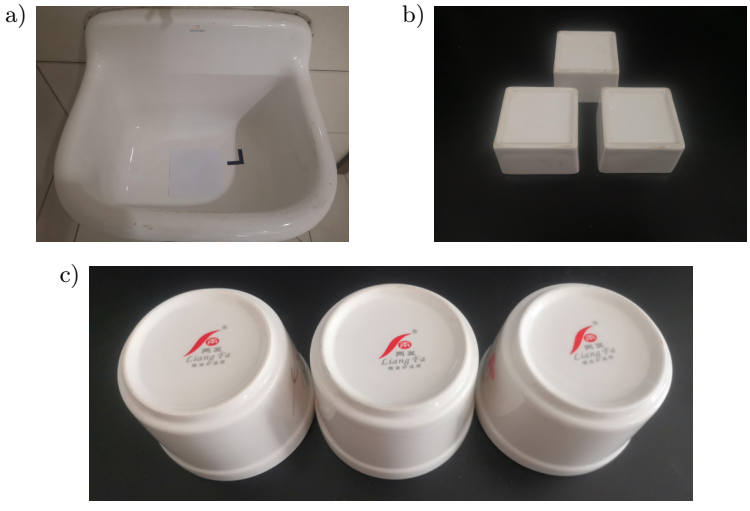

Fig. 8. Additional ceramic samples: a) ceramic sinks; b) ceramic boxes; c) ceramic pots.

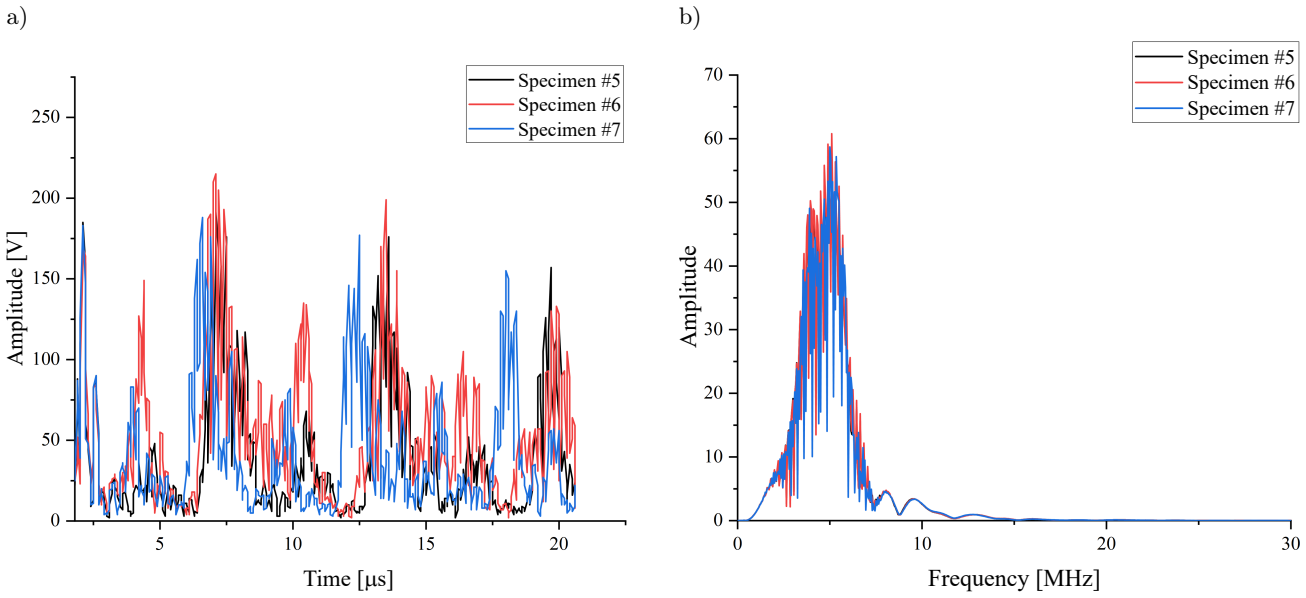

Fig. 9. Time-domain signals and spectra of the ceramic sinks.

Table 5. Target ultrasonic fingerprints of specimen #5.

Domain	Number							
	1	2	3	4	5	...	19	20
Time	4.9865	5.1862	5.0886	5.0006	4.9458	...	6.5132	4.3933
Frequency	43.5764	50.5167	49.7735	50.7363	53.1878	...	55.4088	51.8592

Table 6. Identification of specimen #5 by using ultrasonic fingerprints.

Domain	Number							Threshold
	1	2	3	4	5	6	7	
Time	3.0299	3.4455	4.2011	4.6057	2.7799	2.9915	3.5278	8.1088
Frequency	33.1390	34.4481	42.9251	54.3140	32.4684	33.4754	31.9689	58.9283

Table 7. Identification of specimen #6 by using ultrasonic fingerprints.

Domain	Number							Threshold
	1	2	3	4	5	6	7	
Time	22.7507	25.8529	26.6743	27.4999	28.6314	29.4339	29.7828	8.1088
Frequency	123.8227	128.1348	128.4216	129.5173	135.1324	126.7768	127.1504	58.9283

The ceramic boxes and pots were labeled as 8–10 and 11–13, respectively. The time domain signals and spectra of the ceramic specimens are shown in Figs. 10 and 11.

The ultrasonic fingerprints for the target specimen (#8) are listed in Table 8. The ultrasonic fingerprints to be identified of specimens #8 and #9 are listed in Tables 9 and 10, respectively.

Specimens #8 and #9 are accurately identified as "same item" and "different item", respectively, according to the relationship between the ultrasonic fingerprints and the threshold.

The ultrasonic fingerprints of the target specimen (#11) are listed in Table 11. The ultrasonic fingerprints to be identified of specimens #11 and #12 are listed in Tables 12 and 13, respectively.

Each of the above ceramic specimens was identified correctly during the experiments. Partial ultrasonic fingerprint data have been omitted for brevity. In addition, the ceramic samples were completely replaced with metal samples during the identification experiments. The identification of metal specimens is also accurate, which means the ultrasonic fingerprinting can also be applied to metallic materials.

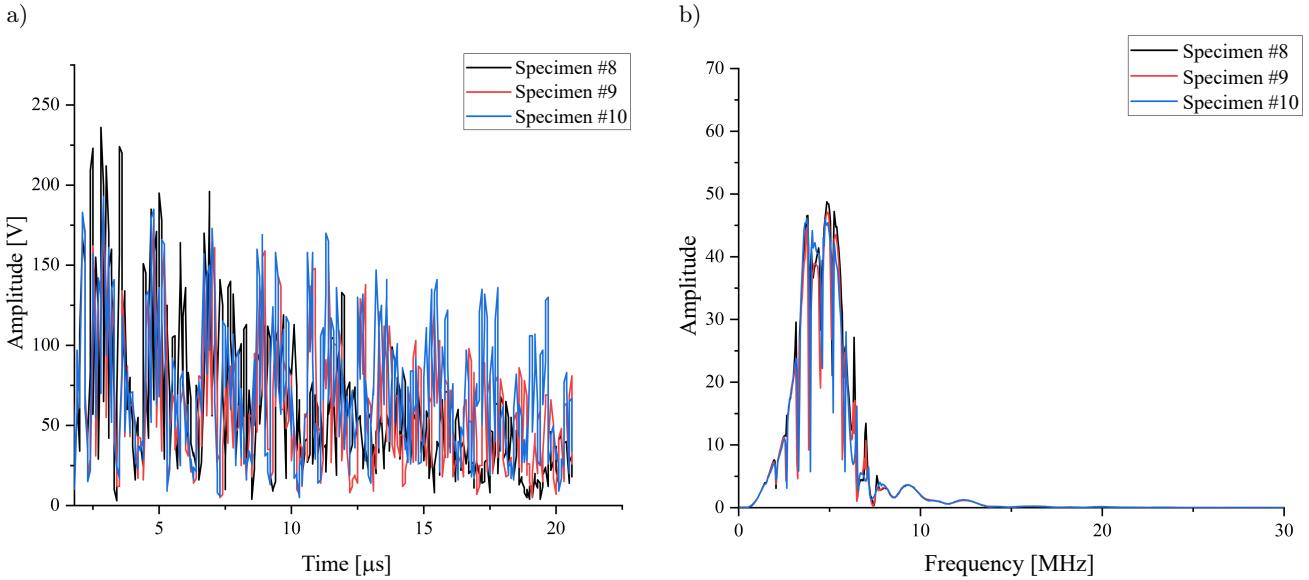

Fig. 10. Time-domain signals and spectra of the ceramic boxes.

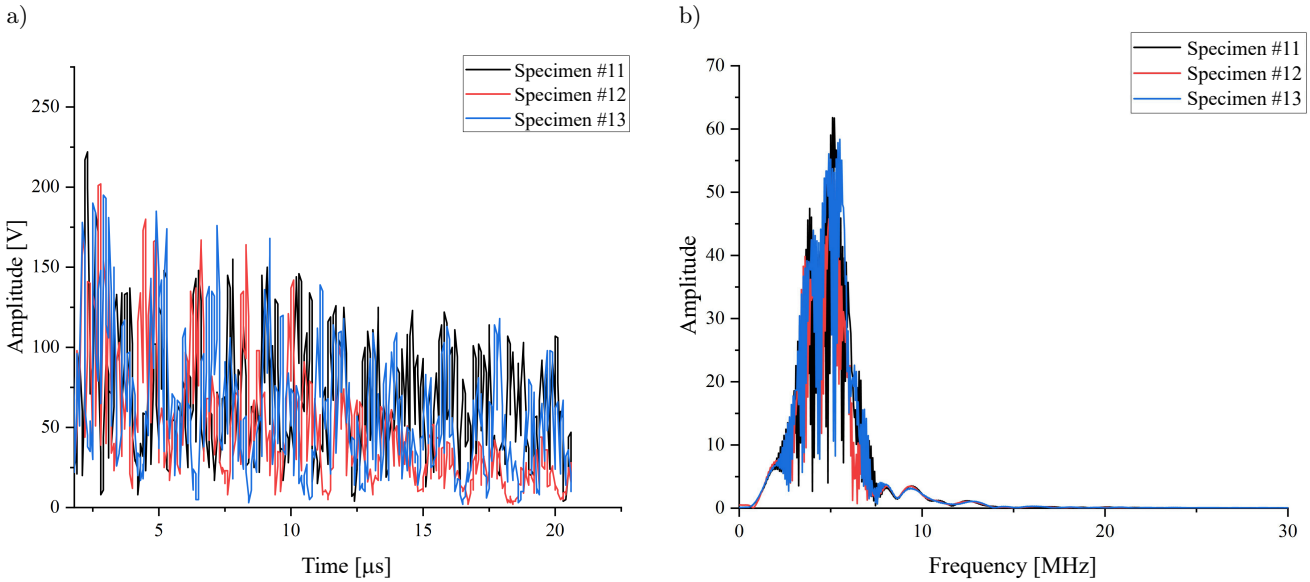

Fig. 11. Time-domain signals and spectra of the ceramic pots.

Table 8. Target ultrasonic fingerprints of specimen #8.

Domain	Number							
	1	2	3	4	5	...	19	20
Time	2.0344	1.1269	1.1505	2.1904	1.3621	...	1.2235	1.1005
Frequency	24.1381	11.4562	11.7572	25.3966	12.2876	...	13.9796	13.7000

Table 9. Identification of specimen #8 by using ultrasonic fingerprints.

Domain	Number							Threshold
	1	2	3	4	5	6	7	
Time	1.3398	1.2174	1.4260	1.5649	1.4916	1.3487	1.2371	2.7580
Frequency	17.2821	14.0739	15.7114	18.2949	14.5042	15.8238	17.0235	21.4454

Table 10. Identification of specimen #9 by using ultrasonic fingerprints.

Domain	Number							Threshold
	1	2	3	4	5	6	7	
Time	5.8814	6.2411	7.1876	7.5086	8.1488	7.5317	7.8776	2.7580
Frequency	60.7242	65.6821	74.9572	78.9511	84.5907	86.5673	88.2513	21.4454

Table 11. Target ultrasonic fingerprints of specimen #11.

Domain	Number							
	1	2	3	4	5	...	19	20
Time	4.1651	3.2998	5.1291	3.2866	3.7905	...	4.0025	4.2389
Frequency	47.9999	31.7008	48.6838	34.2596	38.4055	...	39.5561	47.6875

Table 12. Identification of specimen #11 by using ultrasonic fingerprints.

Domain	Number							Threshold
	1	2	3	4	5	6	7	
Time	3.6012	3.5054	3.1888	3.1953	3.4661	3.3552	3.8833	6.0462
Frequency	31.2349	32.8217	30.9763	31.0628	31.9996	31.7118	39.2756	52.0035

Table 13. Identification of specimen #12 by using ultrasonic fingerprints.

Domain	Number							Threshold
	1	2	3	4	5	6	7	
Time	20.4706	22.0224	24.1944	24.6466	21.3210	23.9550	22.1081	6.0462
Frequency	130.9253	125.4786	128.0756	130.5101	116.5375	132.6178	132.0513	52.0035

5. Conclusions

In this study, the notion of ultrasonic fingerprints was presented to identify and protect ceramics. An algorithm to extract ultrasound signal features was developed as an identification program. The ultrasonic flaw detection card and the computer were assembled into a virtual prototype to integrate the ultrasonic fingerprint acquisition system and the identification system. Then, experiments were conducted to identify a variety of ceramic specimens. The experimental results indicated that the ceramic specimens can be identified and distinguished accurately. The development of the virtual prototype also provides a good foundation for advancing the intelligence, automation, integration, and miniaturization of ultrasonic fingerprint identification systems.

Acknowledgments

This work was supported by the National Natural Science Foundation of China (No. 12174241).

References

1. Badidi B.A., Lebaili S., Benchaala A. (2003), Grain size influence on ultrasonic velocities and attenuation, *NDT & E International*, **36**(1): 1–5, doi: 10.1016/S0963-8695(02)00043-9.

2. Buenos A.A., Jr P.P., Mei P.R., Santos A.A. (2014), Influence of grain size on the propagation of L_{CR} waves in low carbon steel, *Journal of Nondestructive Evaluation*, **33**: 562–570, doi: 10.1007/s10921-014-0252-x.

3. Dejoie C., Tamura N., Kunz M., Goudeau P., Sciau P. (2015), Complementary use of monochromatic and white-beam X-ray micro-diffraction for the investigation of ancient materials, *Journal of Applied Crystallography*, **48**: 1522–1533, doi: 10.1107/S1600576715014983.

4. Figueiredo E., Silva R.J.C., Araújo M.F., Martinez J.C.S. (2010), Identification of ancient gilding technology and late bronze age metallurgy by EDXRF, Micro-EDXRF, SEM-EDS and metallographic techniques, *Microchimica Acta*, **168**: 283–291, doi: 10.1007/s00604-009-0284-6.

5. Hirao M., Aoki K., Fukuoka H. (1987), Texture of polycrystalline metals characterized by ultrasonic velocity measurements, *Journal of the Acoustical Society of America,* **81**(5): 1434–1440, doi: 10.1121/1.394495.

6. Laux D., Cros B., Despaux G., Baron D. (2002), Ultrasonic study of UO_2: Effects of porosity and grain size on ultrasonic attenuation and velocities, *Journal of Nuclear Materials*, **300**(2–3): 192–197, doi: 10.1016/S0022-3115(01)00747-4.

7. Li J., Yang L., Rokhlin S.I. (2014), Effect of texture and grain shape on ultrasonic backscattering in polycrystals, *Ultrasonics*, **54**(7): 178–1803, doi: 10.1016/j.ultras.2014.02.020.
8. Murthy G.V.S., Ghosh S., Das M., Das G., Ghosh R.N. (2008), Correlation between ultrasonic velocity and indentation-based mechanical properties with microstructure in Nimonic 263, *Materials Science and Engineering: A*, **488**(1–2): 398–405, doi: 10.1016/j.msea.2007.11.017.
9. Olinger C.T., Lyon M.J., Stanbro W.D., Mullen M.F., Sinha D.N. (1993), Acoustic resonance spectroscopy in nuclear safeguards, [in:] *34th Annual Meeting of the Institute of Nuclear Materials Management*, https://www.osti.gov/biblio/61350.
10. Özkan V., Sarpün İ.H., Erol A., Yönetken A. (2013) Influence of mean grain size with ultrasonic velocity on microhardness of B_4C-Fe-Ni composite, *Journal of Alloys and Compounds*, **574**(15): 512–519, doi: 10.1016/j.jallcom.2013.05.097.
11. Padeletti G., Fermo P. (2010), A scientific approach to the attribution problem of renaissance ceramic productions based on chemical and mineralogical markers, *Applied Physics A*, **100**: 771–784, doi: 10.1007/s00339-010-5689-x.
12. Palanichamy P., Joseph A., Jayakumar T., Raj B. (1995), Ultrasonic velocity measurements for estimation of grain size in austenitic stainless steel, *NDT & E International*, **28**(3): 179–185, doi: 10.1016/0963-8695(95)00011-L.
13. Sarpün H.I., Kiliçkaya S.M. (2005), Mean grain size determination in marbles by ultrasonic first backwall echo height measurements, *NDT & E International*, **39**(1): 82–86, doi: 10.1016/j.ndteint.2005.06.010.
14. Sciau P., Leon Y., Goudeau P., Fakra S.C., Webbd S., Mehta A. (2011), Reverse engineering the ancient ceramic technology based on X-ray fluorescence spectromicroscopy, *Journal of Analytical Atomic Spectrometry*, **26**(5): 969–976, doi: 10.1039/C0JA00212G.
15. Shi S., Liu Z.G., Sun J.T., Zhang M., Du G.S., Li D. (2015), Study of errors in ultrasonic heat meter measurements caused by impurities of water based on ultrasonic attenuation, *Journal of Hydrodynamics*, **27**: 141–149, doi: 10.1016/S1001-6058(15)60466-8.
16. Smith R.L. (1982), The effect of grain size distribution on the frequency dependence of the ultrasonic attenuation in polycrystalline materials, *Ultrasonics*, **20**(5): 211–214, doi: 10.1016/0041-624X(82)90021-X.
17. Vijayalakshmi K., Muthupandi V., Jayachitra R. (2011), Influence of heat treatment on the microstructure, ultrasonic attenuation and hardness of SAF 2205 duplex stainless steel, *Materials Science and Engineering A*, **529**(25): 447–451, doi: 10.1016/j.msea.2011.09.059.
18. Yang L., Li J., Lobkis O.I., Rokhlin S.I. (2012), Ultrasonic propagation and scattering in duplex microstructures with application to titanium alloys, *Journal of Nondestructive Evaluation*, **31**: 270–283, doi: 10.1007/s10921-012-0141-0.